A study of building vibrations induced by weak motions: effects of earthquake excitation, ambient noise and wind speed

Gaetano Riccio[1,*], Rocco Cogliano[1], Giuseppe Di Giulio[2], Antonio Fodarella[1], Stefania Pucillo[1], Antonio Rovelli[3]

[1] *Istituto Nazionale di Geofisica e Vulcanologia, Grottaminarda, Italy*

[2] *Istituto Nazionale di Geofisica e Vulcanologia, L'Aquila, Italy*

[3] *Istituto Nazionale di Geofisica e Vulcanologia, Rome, Italy*

Article history
Received September 12, 2016; accepted May 12, 2017.
Subject classification:
Building resonance modes, Ambient vibrations, Spectral ratios, Finite element modelling, Ariano Irpino.

ABSTRACT

We carried out a vibration study experiment on a masonry building in the town of Ariano Irpino, southern Italy, using six-channel stations equipped with three-component velocity-transducers and accelerometers and running in continuous modality from January 2006 to December 2007. The analysis of weak motions from several local earthquakes, together with the 3D numerical modelling of the structure, allowed us to identify the first three vibration modes of the target building. Therefore, we checked the validity of ambient noise data to determine the vibration frequencies of buildings. The analysis tools based on earthquake and ambient noise data were conventional, i.e. spectral ratios between homologous components of stations at high floors in the building with respect to a station installed at the basement, and single-station spectral ratios between horizontal and vertical components. The indications derived from earthquakes and ambient noise result in a satisfactory agreement for frequencies between 1 and 20 Hz when using recordings characterized by low levels of amplitude. In contrast, when the wind speed increases (above 20 km/h, approximately) seismic noise shows an excess of horizontal vibrations at low frequencies (below 2 Hz). These extra-amplitudes are not related to the seismic input vertically incident to the basement, but are probably due to the lateral action of the wind on the building. In contrast, anthropic activities do not affect considerably the trend of spectral ratios in the range of frequencies that include the first modes of vibration, even at high noise level.

1. Introduction

Ambient vibrations are largely used in seismology and earthquake engineering to investigate the seismic response of sites. Although limited to the linear behaviour of soils, the information inferred from this typology of seismic signals provides fast and low-cost insight on the buried near-surface structure that also controls ground shaking during earthquakes [for exhaustive reviews see Bard 1999 and Bonnefoy-Claudet et al. 2006]. Ambient vibrations are receiving an increasing attention as valid tools for site classification using simple (1D) geological schemes [Lermo and Chávez-García 1994]. Methods based on ambient noise are also suitable to indicate complex site effects like those due to 2D basin resonances [Fäh et al. 2001], topographic irregularities [Panzera et al. 2011] and cavities [Panzera et al. 2013], oriented cracks in fault zones [Rigano et al. 2008, Di Giulio et al. 2009, Pischiutta et al. 2012 and 2013], and unstable rock slopes [Burjánek et al. 2010 and 2012].

A brief description of the pioneering studies using ambient noise in the dynamic building response can be found in Kotronis et al. [2013]. Many experimental works show the reliability of ambient vibration measurements in engineering applications in assessing the fundamental resonances and the mode shapes of the target structure [Fäcke et al. 2006, Gallipoli et al. 2009, Oliveira et al. 2010, Michel et al. 2010, Herak and Herak 2010, Masi et al. 2010]. The availability of a continuous source of excitation is indeed very attractive: ambient vibrations permit a fast statistical approach to study building resonant frequencies in short measurement times and with low costs [Parolai et al. 2005, Mucciarelli and Gallipoli 2007, Ivanovic et al. 2000]. In civil engineering, the modal parameters of target structures are usually estimated using the Frequency Domain Decomposition (FDD) technique [Brincker et al. 2001, Ventura et al. 2003, Michel et al. 2007, Gentile and Saisi 2007, Guéguen et al. 2012, Bindi et al. 2015] or similar "output only" techniques. FDD is

based on Singular Value Decomposition (SVD) of the cross-power spectral density matrix using simultaneous recordings of seismic noise. Recent applications shows that FDD can provide the modal shape also in geological environments; Guéguen et al. [2011] studied the modal shape of a 1-D soil profile using borehole seismic stations, Poggi et al. [2015] assessed the resonance characteristics of a 2-D sedimentary basin.

However among engineering studies, not so many efforts have been devoted so far to check the role of the different vibration sources (traffic, industries, meteorological factors) and to investigate variations in building excitation between dynamic perturbations induced by sources situated inside or outside the buildings.

In this paper, we use ambient noise data and low-magnitude earthquake signals recorded on a test building in the town of Ariano Irpino, southern Italy, with the goal of the determination of its main resonance modes. The test structure is a building of architectural interest for Italy, being made of reinforced concrete and masonry. It was built in the early 1950's but is still representative of the national-socialist style typical of the previous two decades. The interest for this building is also due to its housing of strategic and decisional offices that are responsible for coordinating seismic emergency activities at local and regional level. The building is situated in the central square of the town that is the traditional meeting place for the residents.

Standard spectral ratios, henceforth SSRs, between receivers at different floors and a reference station installed below the ground level are used to compute transfer functions along vertical profiles in the building. The dynamic identification of several lowest order resonances is performed using conventional finite element modelling. The first two orthogonal vibration modes and a torsion mode are well identified in spite of the small (2-storey) height of the test building. We have then compared at each receiver both resonant frequencies and transfer functions derived from earthquakes and ambient vibrations, selecting time periods with ambient vibrations characterized by both anthropic and meteorological origin. Indeed many published works evidenced a strong correlation between amplitude of the seismic noise and meteorological condition [Kohler et al. 2005, Clinton et al. 2006, among many others]. We have found that transfer functions derived from ambient noise are more consistent with those computed from earthquake records when calm (by night) seismic background is used and meteorological perturbations are weak. Internal and external localized sources in hours of the day and laterally pressing gusts of wind may change the building excitation mechanisms causing a different distribution of energy among the predominant modes. A warning rises for fast measurements using one receiver only on the top of buildings: results can be significantly biased especially when ambient vibration measurements are contaminated by strong meteorological and internal anthropic disturbances.

2. The test building

The study building is located on the top of a hill having sharp variation in altitude (Figure 1a). Foundation soil consists of alternating layers of cemented and weakly cemented sand, interspersed with layers of gray clay (Figure 1a). To compensate for the local altitude variation, the building has a single underground floor on the north-west side and three underground floors on the north-east side. The building has a typical C shape, dimensions of 30.55 x 24.30 m with two floors above ground (Figure 1b). The vertical load-bearing structure of floors above ground is made of solid brick masonry, whereas it is made of stone masonry in the ground floor and floors below ground. The horizontal structure is made of mixed cast-in-place reinforced concrete slabs and semi-hollow tile blocks. Floors are joined to the vertical structure by reinforced concrete string-courses.

Since January 2006 seven seismological stations were installed in the building. Each station consists of a Quanterra Q330 digitizer with hard drives for data recording, equipped with three-component velocity-transducers (Le3D-5s manufactured by Lennartz) and accelerometers (Episensor by Kinemetrics). Accelerometers were fixed to the floors, while velocimeters were just leaning on them. Six-channel records were collected in continuous modality in the periods January to March 2006 and June to December 2007. Between April 2006 and May 2007, only three-component accelerometers were recording. Velocity transducers have flat amplitude response between 0.2 and 50 Hz, 140 dB dynamic range and are characterized by very low electronic noise (rms < 1 nm/s at 1 Hz); accelerometers have 155 dB dynamic range and their full scale range was set to 1g. For ambient noise analysis we used recordings from velocity-transducers, which are less noisy than accelerometers especially at low frequencies.

The station positions at the different floors are

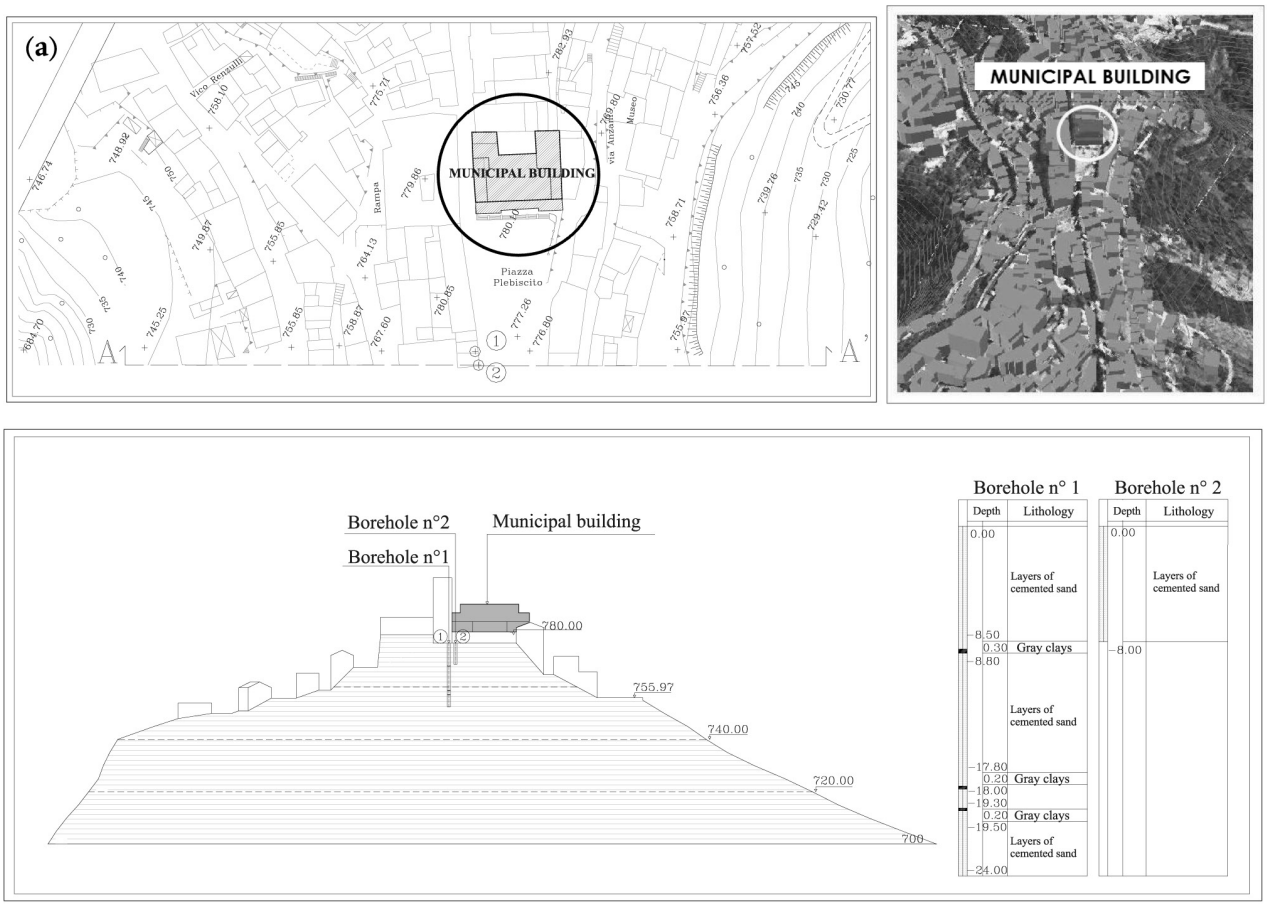

Figure 1a. The upper part shows a map of the area where the Municipal building stands, and a Google view of the topography. Numbers 1 and 2 indicate the location of two available geological bore-holes. The lower part shows a vertical section conducted along line A-A' in the left side, and the vertical geological profile in the right side.

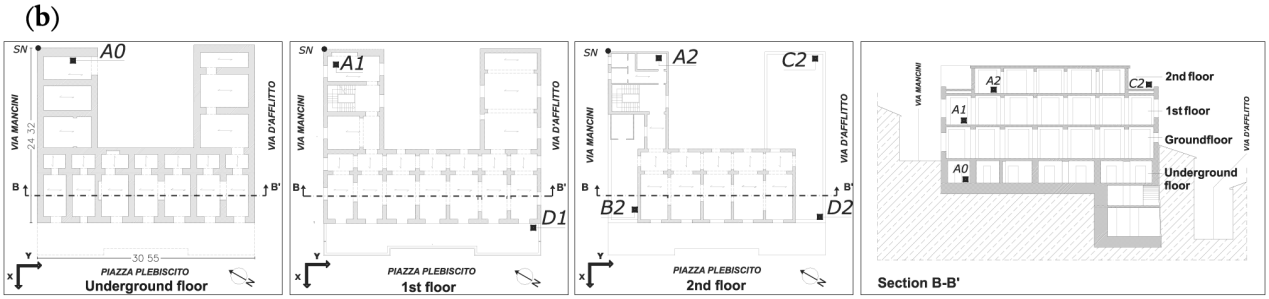

Figure 1b. From the left: The first three panels show a scheme with the detail of each floor, together with the position of the stations at the various levels. The reference station A0 was installed at the basement, below the ground level; stations A1 and D1 at the first floor; stations A2, B2, C2 and D2 at the second floor. The panel in the right side shows the vertical section of the building along line B-B' shown in the previous three panels.

shown in Figure 1b. One station was used as a reference (A_0): it was placed on the lowest level underground floor of the north-east side and was assumed as being representative of the incident seismic input. Stations A1 and D1 were placed at the first floor, in correspondence of the northern and southern edge of the building respectively; the remaining stations, A2, B2, C2 and D2, were placed at the four edges, approximately, of the second floor. All stations were arranged with the two horizontal components oriented along the minor and major side of the building (represented as x and y, respectively, in Figure 1b). Further details about instrumentation and installation can be found at http://www.gm.ingv.it/index.php/sismologia-e-ingegneria-sismica/ricerca-scientifica/13.

Signals were continuously recorded with a sampling rate of 100 Hz, producing about 2 GB of data (miniseed format) per month per station. Each station was equipped with a GPS antenna for time synchronization.

3. Earthquake data and analysis

During the acquisition period (January 2006 - December 2007), stations recorded hundreds of earthquakes at local and regional distances. Twenty of them, listed in Table 1, were selected on the base of a satisfactory signal-to-noise ratio, their epicentres are shown in Figure 2. We applied a selection criterion requiring that the Fourier amplitude spectrum, henceforth FAS, of the earthquake signal exceeds the FAS of noise by more than a factor of 3 in the investigated frequency band (1-20 Hz). The signal spectrum is calculated in a time window bracketing the most significant portion of the earthquake signal including the first arrival of S-waves and early coda. To calculate the noise spectrum we used a window of seismic noise preceding the direct P wave of earthquakes, with the same duration of the window used for the earthquake signal. Among the recorded earthquakes, the signal-to-noise > 3 criterion is met for sixteen events in the band 1-10 Hz, and only for four events in the band 1-20 Hz.

The local magnitude (M_L) of selected events, taken from the seismic bulletin of Istituto Nazionale di Geofisica e Vulcanologia (INGV), is comprised between 1.5 and 4.8 and epicentral distances range from 4 to 116 km (Table 1 and Figure 2). More detailed information is available at http://bollettinosismico.rm.ingv.it. Figure 3 shows the comparison, for an example event, between the waveforms recorded by the reference station A_0 and those recorded by stations A1 and A2, placed on the same vertical of A_0 at the first and second floor, respectively. Seismograms show increasingly larger amplitudes of the horizontal components with increasing height, whereas the vertical components are substantially unchanged.

The recorded data were analyzed using conventional spectral techniques yielding transfer functions [Fäcke

#	Lat	Lon	Depth (km)	M_L	Date	Time	R (km)	PGAe (m/s^2)	PGAn (m/s^2)	PGVe (m/s)	PGVn (m/s)	Stations	Sensors
1	40.981	15.151	13	2.4	11/01/2006	08.28.52	20	5.82E-04	5.48E-04	1.40E-05	2.01E-05	3	A-V
2	41.114	14.939	10	1.8	05/02/2006	15.08.19	13	9.22E-04	1.01E-03	2.89E-05	4.82E-05	4	A-V
3	40.789	15.220	10	3.2	05/02/2006	17.02.59	42	2.16E-03	1.66E-03	7.25E-05	7.73E-05	4	A-V
4	40.796	15.322	9	2.7	14/03/2006	03.15.03	44	2.23E-04	4.01E-04	1.26E-05	2.25E-05	6	A-V
5	40.860	15.340	11	1.6	14/03/2006	03.50.11	39	4.64E-04	3.87E-04	6.44E-06	6.90E-06	6	A-V
6	41.710	16.021	29	3.3	14/04/2006	01.21.59	100	4.94E-04	5.29E-04	1.53E-05	2.42E-05	6	A
7	41.467	15.699	6	3.0	30/04/2006	21.07.57	62	6.24E-04	9.89E-04	2.37E-05	4.63E-05	7	A
8	41.801	15.903	31	4.8	29/05/2006	02.20.06	99	1.52E-02	1.55E-02	1.52E-02	1.55E-02	7	A
9	41.142	15.040	11	1.5	23/07/2006	02.29.04	40	3.02E-04	3.32E-04	7.41E-06	8.66E-06	7	A
10	41.957	15.490	6	3.8	06/08/2006	19.33.31	95	1.80E-03	2.02E-03	8.58E-05	8.91E-05	7	A
11	41.166	15.273	17	2.2	14/08/2006	11.11.37	16	1.06E-03	1.03E-03	3.00E-05	3.81E-05	7	A
12	42.074	15.746	37	4.2	04/10/2006	17.34.20	116	1.37E-03	2.54E-03	7.92E-05	1.09E-04	7	A
13	41.718	15.771	18	2.1	23/10/2006	02.23.51	85	1.44E-04	1.94E-04	1.85E-06	2.40E-06	7	A
14	41.147	14.926	9	2.1	05/03/2007	01.37.32	14	1.07E-03	1.36E-03	6.07E-05	6.11E-05	6	A
15	41.228	15.074	18	1.8	05/04/2007	00.03.00	8	5.16E-04	6.12E-04	1.01E-05	2.16E-05	6	A
16	41.184	15.087	19	2.0	05/04/2007	00.08.43	4	6.71E-04	1.16E-03	2.27E-05	4.77E-05	6	A
17	41.189	15.072	18	1.8	05/04/2007	01.00.47	4	2.86E-04	4.02E-04	7.53E-06	1.55E-05	6	A
18	41.101	14.875	10	2.1	20/06/2007	07.08.48	19	1.17E-03	1.37E-03	3.52E-05	4.32E-05	6	A-V
19	41.420	15.849	2	3.6	10/07/2007	11.55.00	70	5.09E-04	6.29E-04	1.75E-05	2.94E-05	6	A-V
20	41.700	14.810	22	4.0	18/10/2007	23.25.45	65	3.58E-03	4.83E-03	1.90E-04	2.49E-04	6	A-V

Table 1. List of earthquakes analyzed in this study and values of peak acceleration and velocity recorded at the reference station. Information in the columns 2 to 7 is taken from the seismic bulletin of INGV.

#: Sequential number as shown in Figure 2
Lat, Lon and Depth: Coordinates of the earthquake -hypocentres
M_L: Local magnitude
Date and Time : Date and time of the earthquake
R: Epicentral distance from Ariano Irpino
PGAe: Maximum acceleration recorded at the basement on the E-W component (x side)
PGAn: Maximum acceleration recorded at the basement on the N-S component (y side)
PGVe: Maximum velocity recorded at the basement on the E-W component (x side)
PGVn : Maximum velocity recorded at the basement on the N-S component (y side)
Stations: Number of stations that recorded the earthquake
Sensors: Sensor type (A accelerometer, V velocimeter)

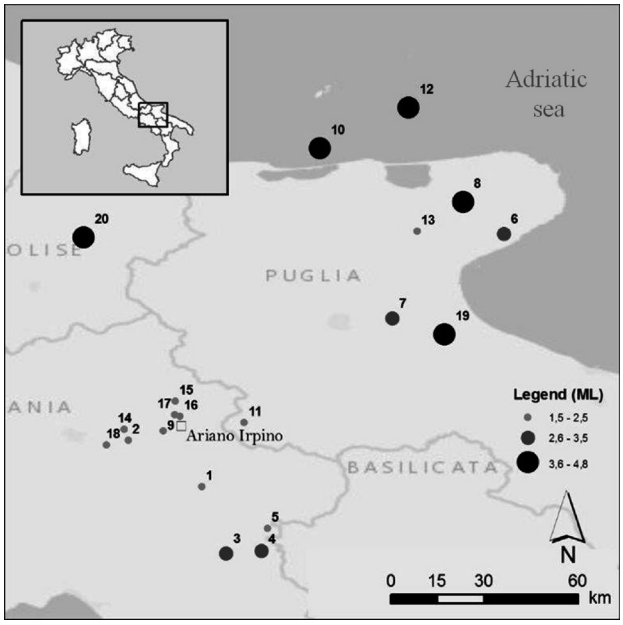

Figure 2. Map showing the epicentres of the earthquakes used in the analysis (see Table 1).

et al. 2006]. Such techniques are widely used in seismological studies [Borcherdt 1970, Tucker and King 1984] to compute experimental transfer functions among stations installed on different geological formations. The application of SSR technique is more limited in building response analysis [Celebi and Safak 1991, Fäcke et al. 2006] where the H/V (horizontal-to-vertical) spectral ratio [Nakamura 1989] is preferred. SSRs indeed require a hard-rock reference station to compute the amplification of the other sites relatively to that reference. In our case study, we assume that the recorded signal at the basement (A0) of the building is the reference input representative of the incident seismic radiation. This approximation is acceptable under the assumption that soil-structure interaction is negligible [Trifunac et al. 2001, Kotronis et al. 2013]. Our target building is assumed as a flexible structure on rigid soil [fixed-base; Guèguen et al. 2017], and then the foundation motion is expected the same of the ground. This *a priori* hypothesis is crucial for the reliability of the results, and will be discussed later on.

The transfer function of the generic station A_n is (by definition) given by the Equation (1)

$$H_n(f) = \frac{FFT[A_n]}{FFT[A_0]} \quad (1)$$

where FFT means Fast Fourier Transform. In seismological studies, transfer functions are preferentially computed by calculating SSR between the FASs on the single events (or noise windows) and then averaging over individual ratios, whereas in engineering studies the cross-spectra are more widely used; in this case the transfer function is evaluated as $C_{n0}(f)/C_{00}(f)$, where C_{n0} denotes the average (over all events or noise windows) cross-spectrum between the generic n-station and the basement station, C_{00} denotes the basement average auto-spectrum of the reference station. The cross-spectrum approach assumes equal distribution of energy in the frequency band of analysis, then in our case the first approach based on FFT ratios is more suitable because the selected earthquakes have very different energy spectra.

Transfer functions based on ratios of Fourier Spectral Amplitudes are calculated separately at the different stations for each of the selected events and for each component of motion. Therefore, geometric mean and statistical uncertainties (± 1 standard deviation) are computed averaging over all the events. The average trend of stations is shown in Figure 4 column I; in Figure 4 column II the ± 1 s.d. band of two stations that show small (A1) and large (B2) amplification respectively gives insight on the range of uncertainties of our estimates.

The first peak of SSRs (Figure 4 column I), which is fairly well evident for all of the building stations, is between 5 and 6 Hz and characterizes the building vibration mostly in the y direction. The largest amplitude (more than a factor of 10 compared to the reference station) is reached at a frequency between 5 and 6 Hz for the two stations B2 and D2 of the top floor. This suggests that it is the fundamental mode of oscillation along the major side of the building.

However, the height is not the only factor that affects vibration amplitudes: station D1, located at the first floor, shows an amplification higher than stations A2 and C2, which are at the second floor. The first peak of SSRs for the x component is found at the same frequency of the y component (between 5 and 6 Hz), but the greatest amplification is reached between 7 and 9 Hz.

To identify more accurately the predominant motion directions, the average SSRs were also computed by performing a rotation of the two horizontal components from 0° to 180° using bins of 5°s. Directions of 0° and 90° correspond to x and y, respectively. The contour plots obtained for the rotated components are shown in Figure 5a for the stations at the top floor. We see that the 90°-polarized (transversal) spectral peak at 5.75 Hz and the 0°-polarized (longitudinal) spectral bump between 7 and 9 Hz, previously identified, are quite clearly uncoupled to each other both in frequency and direction, so they likely represent the first two translational vibration modes. A difference in amplitude between the station couples A2-C2 and B2-D2 is evident. A possible origin

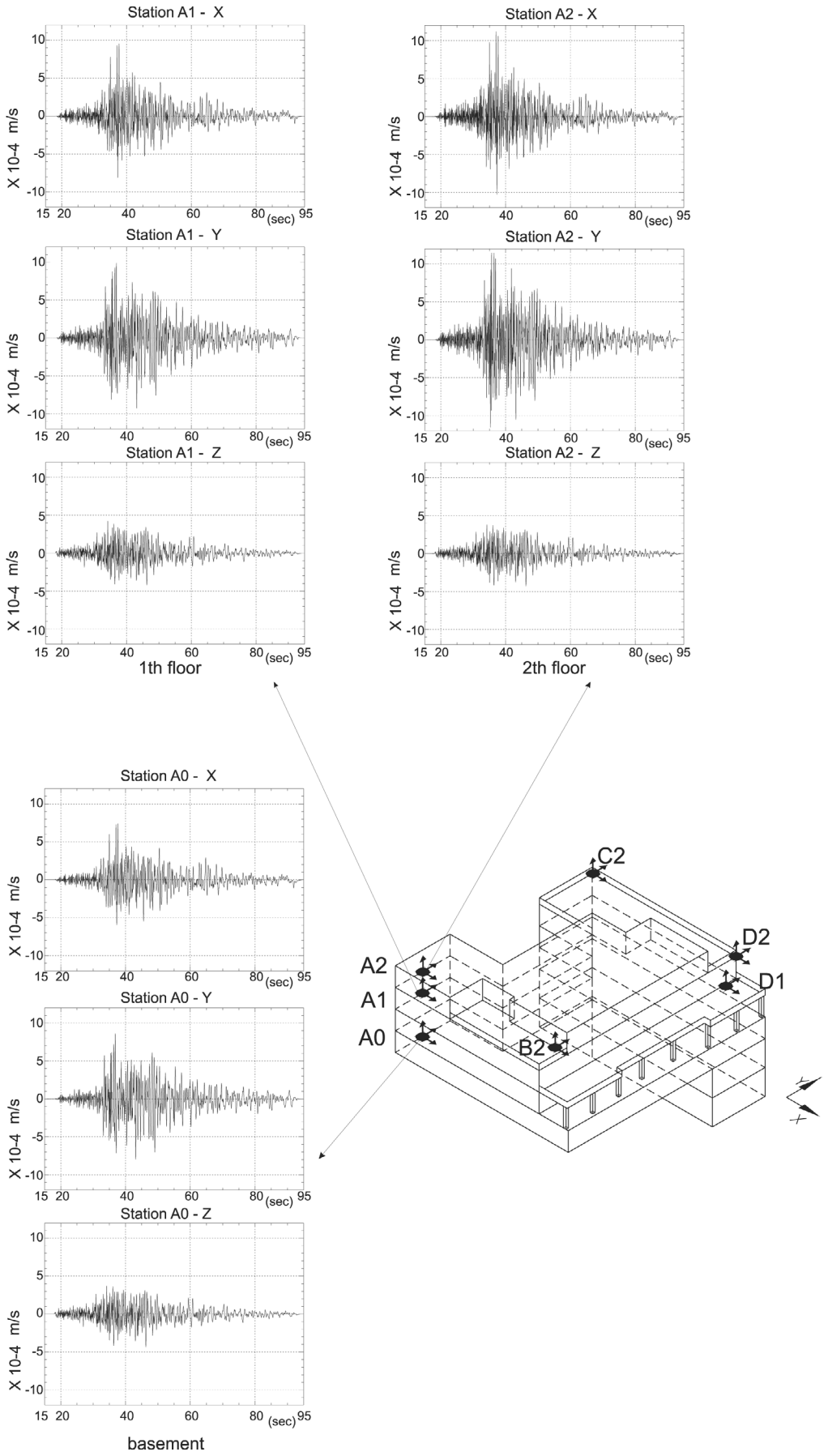

Figure 3. Velocity waveforms recorded by the stations A0, A1 and A2, placed on the same vertical line, during the M_L 4.8 earthquake of May 29, 2006.

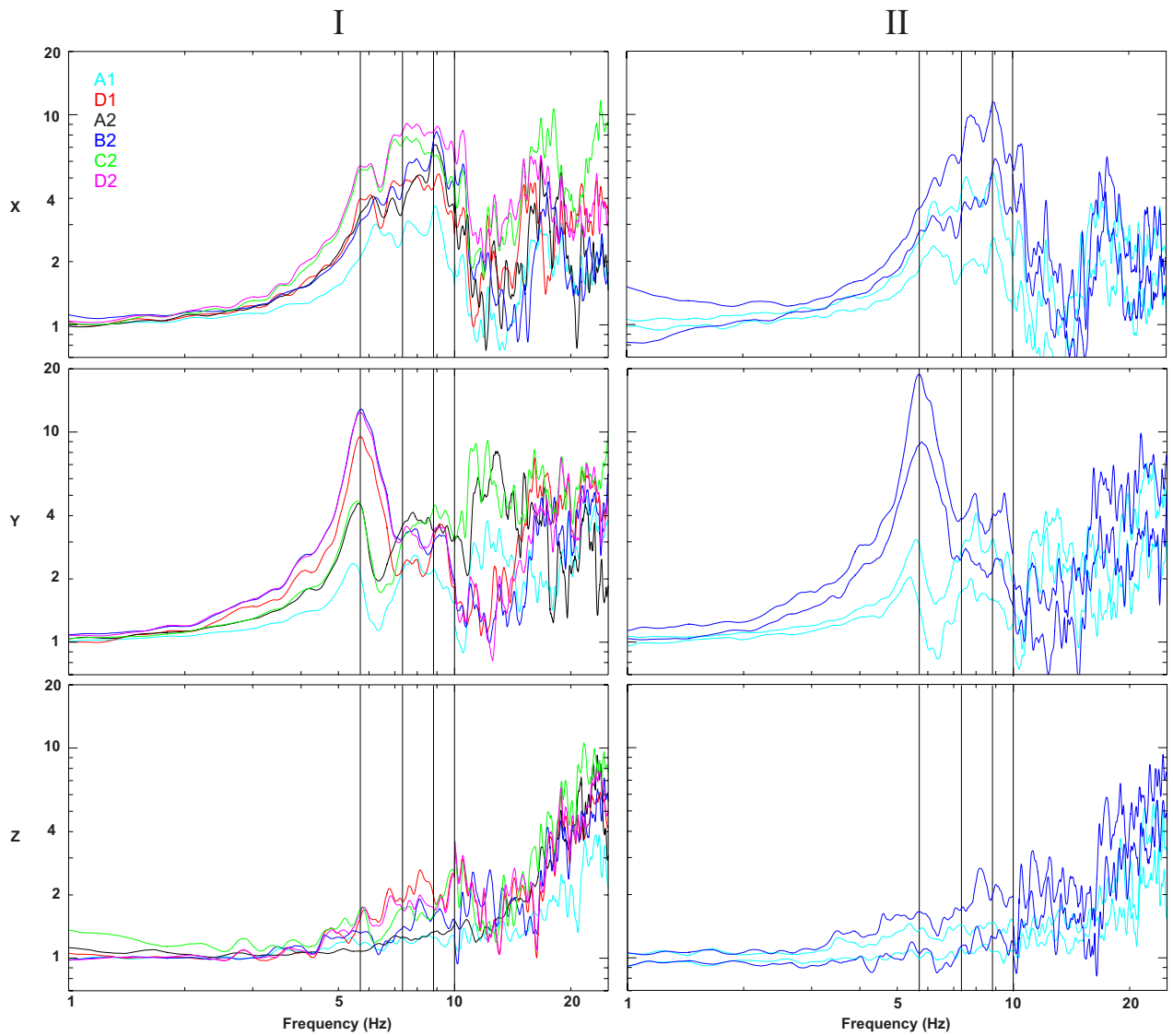

Figure 4. Column I): Spectral ratios for the three components of motion in the building with respect to the reference station, obtained by averaging over twenty earthquakes in the frequency band 1-10 Hz. Gray vertical lines indicate the frequencies of the vibration modes outlined by the numerical modelling. The curves between 10 and 25 Hz were calculated using only the four earthquakes for which signal to noise ratio exceeded the threshold of 3 up to 25 Hz. (Column II) ± 1 standard deviation bands of two stations in the building that show small (A1, light blue) and large (B2, dark blue) amplification respectively.

of this difference will be discussed in the conclusions.

SSRs of vertical components (Figure 4 column I) are essentially flat up to 5-6 Hz, and amplifications remain low (< 3) up to 15 Hz, approximately. Between 20 and 25 Hz, vertical motions show large amplification relative to the basement, with a trend roughly common to all stations. In contrast, horizontal components show a larger variability for $f > 10$ Hz, especially along the y direction.

4. Identification of vibration modes

To interpret the spectral peaks of experimental data in terms of vibration modes, we constructed a three-dimensional model of the building simulating the building excitation under seismic actions. We applied the finite element program SAP2000 (https://www.csiamerica.com/products/sap2000) that performs eigenvectors modal analysis in the linear range and determines the modal deformations of free undamped vibrations. We used two-dimensional elements of the "shell" type for the geometric discretization of the vertical structure (made of stones and solid bricks), internal fillings (hollow bricks) and string-courses (reinforced concrete). The floors at various levels of the building were supposed to have infinite stiffness and to transmit a vertical line load to the walls below. The numerical model is composed of about 17700 nodes and 9100 shells (Figure 6).

We used mechanical parameters listed in Table 2. The specific weight γ and the Poisson's ratio ν were fixed for each type of material, whereas the elasticity modulus E is varied within intervals according to

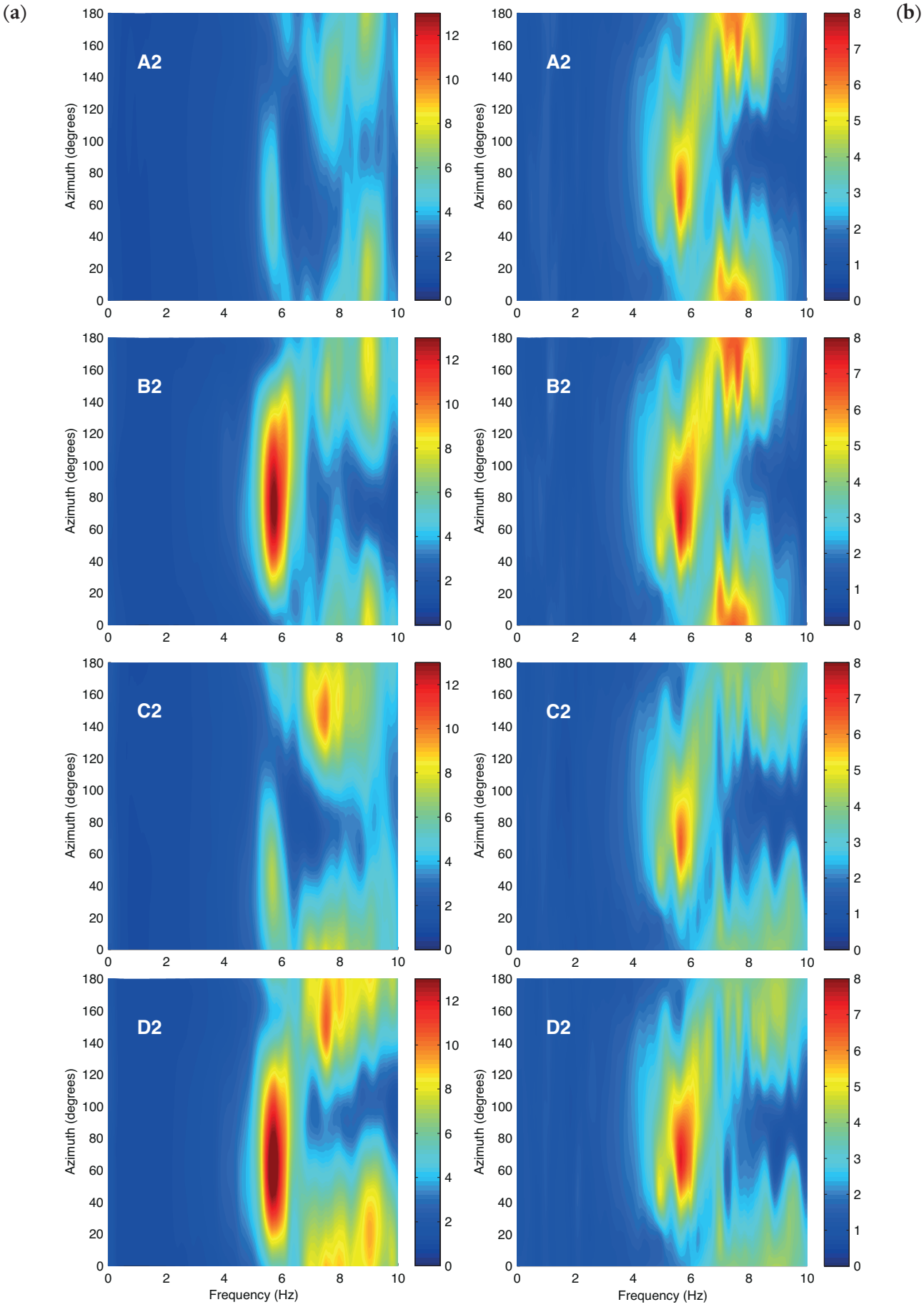

Figure 5. Contour plots of the four stations installed on the top floor, obtained by computing spectral ratios on rotated (from 0° to 180° at bins of 5°) horizontal components: (**a**) average spectral ratios on earthquakes, (**b**) spectral ratios computed from synthetic seismograms of the best fit model using the M_L 4.8, 29 May 2006 earthquake.

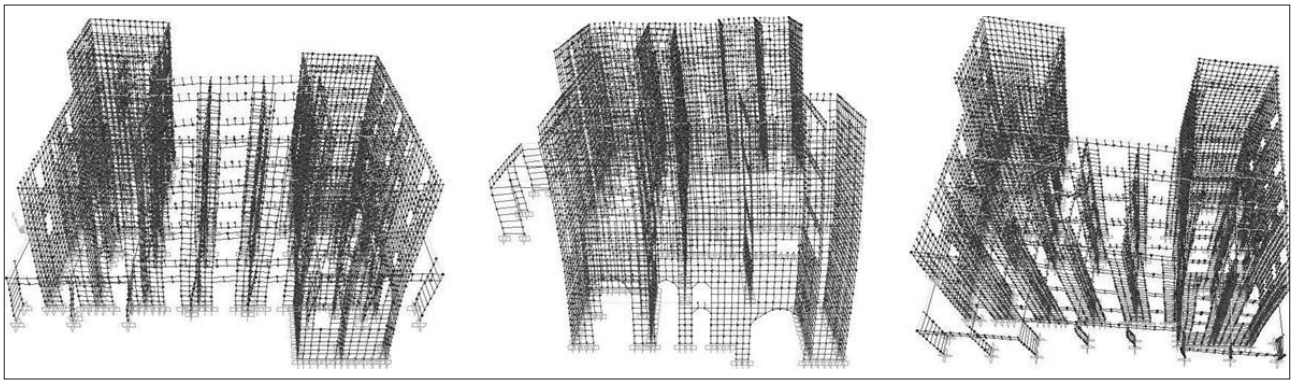

Figure 6. Modal shapes of the first 3 vibration modes; the first two are translational along y and x direction respectively, the third is rotational. Animations of these vibration modes can be found at http://www.gm.ingv.it/index.php/sismologia-e-ingegneria-sismica/ricerca-scientifica/13-13.

standards prescribed by the Italian seismic code [NTC 2008]. The value of shear modulus G is then given by

$$G = \frac{E}{2(1+\nu)} \qquad (2)$$

We performed some preliminary tests by varying E (and G) of the RC string-course within the expected variability interval (Table 2). Since we observed that these variations affect only slightly the results of modelling, we decided to fix the elastic modulus of reinforced concrete (E = 24500 N/mm^2). The elastic modulus of hollow bricks was fixed as well. We then looked for an optimal value of E of stones and solid bricks in a least squares approach. The variability intervals of E reported in Table 2 were sampled with bins of 2000 Kg/cm^2 (about 196 N/mm^2); for each couple of elastic moduli of the two materials the frequencies of the vibration modes were evaluated through numerical modelling. The cost function was constructed as the sum of the squared differences between the experimental spectral peaks (f_j^{obs}) and the theoretical vibration frequencies (f_j^{mod}), and was computed considering the first three vibration modes. The cost function is then given by

$$\varepsilon = \sum_j (f_j^{mod} - f_j^{obs})^2 \qquad j = 1,2,3 \qquad (3)$$

The values of the experimental frequencies f_j^{obs} selected in Equation (3) are those of the peak of the SSR with the largest amplitude for the first three modes in Figure 4 column I:

$$f_1^{obs} = 5.75 \text{ Hz}$$
$$f_2^{obs} = 7.80 \text{ Hz}$$
$$f_3^{obs} = 8.95 \text{ Hz}$$

The values found for the elastic moduli of the best model (in a least-mean-square criterion) are given in parentheses in Table 2.

Finally, we investigated the dynamic behaviour of the building using the parameters that minimized the misfit function ε. Numerical modelling yields nine vibration modes that have resonance frequency within the frequency range investigated with experimental data. Table 3 shows the values of the percentage of modal participating mass of the translational (UY, UX, UZ) and rotational components (RY, RX, RZ). The percentages of modal participating mass give an estimate of the single mode contribution to the response to the loads of acceleration along each of the three directions of motion [Cook et al. 1989].

Table 3 confirms that the translational motions along y and x directions are predominant for the first and second mode, respectively, whereas the third mode is characterized mainly by rotation around the z-axis. Figure 6 shows the deformation of the structure for these three modes.

The first mode returned by the numerical model is characterized by a frequency f = 5.75 Hz, in

Type of material	Specific weight γ (KN/m^3)	Elasticity Modulus E (N/mm^2)	Poisson's ratio ν
Brick masonry	17.6	2800-3400 (3330)	0.25
Stone masonry	20.5	2600-3200 (2940)	0.25
Reinforced concrete curb	23.5	(24500)	0.25
Hollow bricks	11.8	4400	0.25

Table 2. Properties of the materials used in the modelling. The column "Elasticity Modulus" shows the range over which the parameter was varied in the numerical models (numbers in parentheses are the best fit values).

Mode	Period (s)	Frequency (Hz)	UY (%)	UX (%)	UZ (%)	RY (%)	RX (%)	RZ (%)
1	0.1739	5.75	51	0	0	0	1	7
2	0.1337	7.48	0	43	0	2	0	5
3	0.1120	8.93	0	7	0	0	0	27
4	0.0655	15.25	10	0	0	0	4	2
5	0.0569	17.56	0	9	0	4	1	2
6	0.0553	18.06	0	0	39	11	40	0
7	0.0517	19.32	0	0	7	1	0	0
8	0.0508	19.68	1	0	0	4	3	3
9	0.0488	20.47	0	0	10	15	4	1

Table 3. List of the first nine vibration modes, and percentage of participating modal masses obtained in the numerical modelling (values greater or equal to 5% are highlighted in gray).

good agreement with the observed one, and a participant mass equal to 51% (Table 3). The modal deformation of the numerical model (Figure 7) and the distribution of participating mass confirms that it is a translational mode along the y direction. The experimental data (Figure 4 column I, y direction) consistently show a clear peak of the SSRs between 5.55 Hz (station A1) and 5.80 Hz (station D2).

This range of variability is shown in Table 4 for all the resonance frequencies assessed experimentally. The second mode affects mostly the x direction, with a participant mass equal to 43%. Its modal deformation still reveals a mainly translational mode even if the numerical model returns also a contribution of about 5% of the participating mass to the rotational deformations around the vertical axis (Table 3).

Its frequency of vibration in the model is f = 7.48 Hz. Also for this mode, the range of frequencies found experimentally for the spectral peak in the x direction is in good agreement with the value obtained in the numerical simulations (Table 4). The third mode returned by the model is characterized by a frequency f = 8.93 Hz with a participating mass of 7% and 27% for the deformation along the x direction and rotation around the z axis, respectively (Table 3).

Above the third mode, the participating mass returned by the model is still important (Table 3) but the identification of the amplification band in the experimental data is more complex. It is interesting to note that, above 17 Hz, amplification of the vertical component is present both in experimental data (z direction in Figure 4 column I) and in numerical models (Table 3, from the sixth to the ninth mode).

A preliminary test (not shown here) using the FDD technique returns peaks in the singular values of the power spectral density matrix [computed following Welch 1967] at 5.60, 8.00 and 8.95 Hz. These values are in good agreement with the frequencies of the SSR peaks (Table 4). The modal shape associated to the singular vector at these three frequencies confirms the mode of oscillation inferred from the numerical modeling.

The consistency of results between FDD and SSR method is a first confirmation that the role of soil-structure interaction is negligible and does not bias the resonant frequencies in our SSR estimate. Further arguments will be provided later on, when the spectra at the basement are analyzed for different sources of excitation.

Vibration modes		Experimental		Numerical (initial model)		Numerical (best fit model)	
		Freq. (Hz)	Periods (s)	Freq. (Hz)	Periods (s)	Freq. (Hz)	Periods (s)
1st	translational (y-direction)	5.55-5.80	0.1801-0.1724	5.44	0.1837	5.75	0.1739
2nd	translational (x-direction)	7.65-7.95	0.1307-0.1257	7.06	0.1415	7.48	0.1337
3rd	rotational (x-y plane)	8.90-9.20	0.1123-0.1087	8.41	0.1189	8.93	0.1120
4th	translational (y-direction)	11.70-13.00	0.0854-0.0769	14.31	0.0699	15.25	0.0655
5th	translational (x-direction)	16.00-18.20	0.0625-0.0549	16.50	0.0606	17.56	0.0569
6th	rotational (y-z plane)	21.00-22.50	0.0476-0.0444	17.03	0.0587	18.06	0.0553

Table 4. The main vibration modes resulting from experimental data are compared to results from numerical modelling. The values shown for the initial model correspond to the lower limit of the variability range of the elastic moduli in Table 2.

(a)

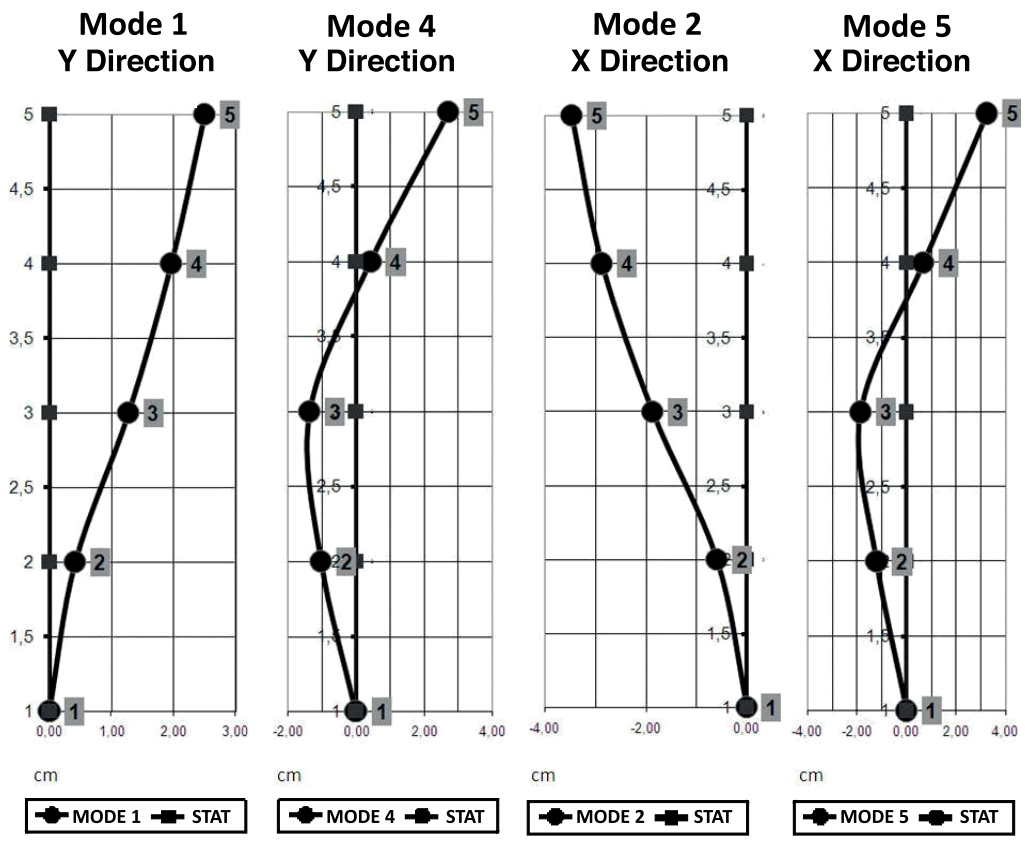

(b)

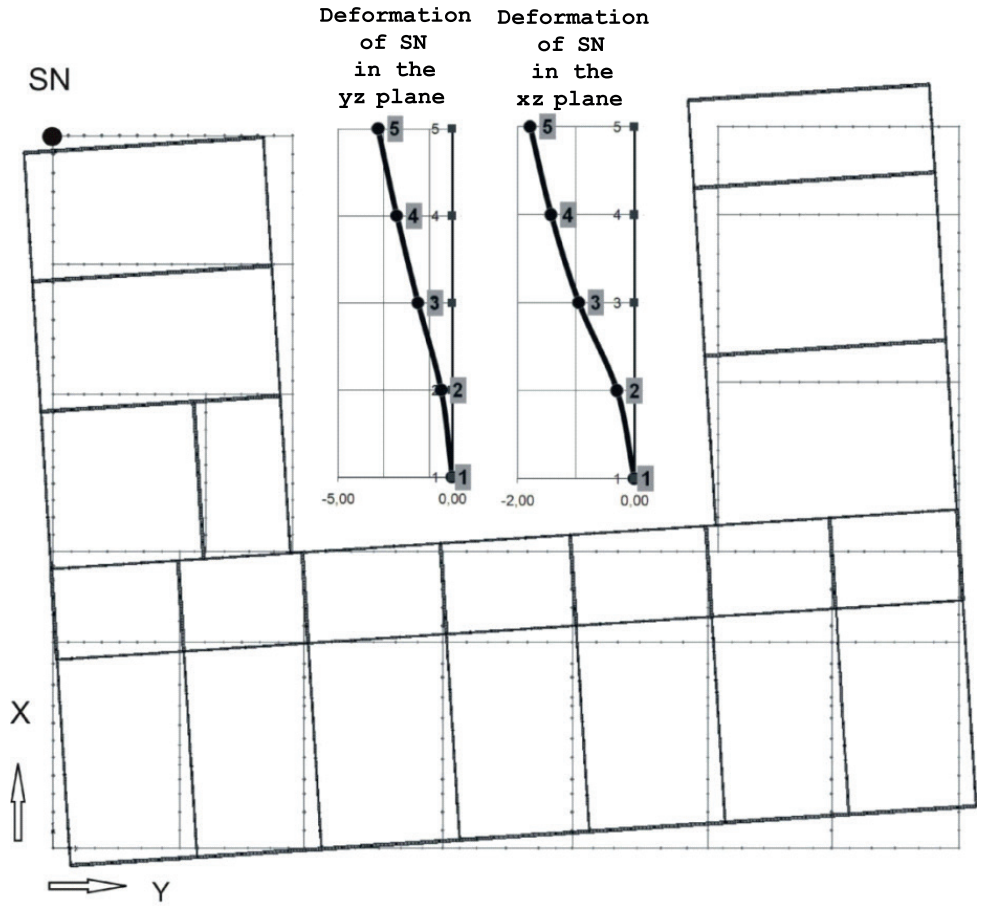

Figure 7. (a) Mode shapes on the vertical profile in the northern edge of the building (the SN point in Figure 1b). The ordinates represent levels of the building according to the model grid discretization , the abscissas are the displacements of the mode shapes normalized to unity modal mass. (b) Deformation in the xy plane relative to the third mode. The deformations in xz and yz planes are also shown for the SN point.

5. Ambient vibrations

Ambient noise of anthropic and meteorological origin had been known since long time to affect the frequency band above 1 Hz, where the main vibration modes of historical buildings generally fall. Meteorological perturbations also increase ambient noise at low frequencies (f <1 Hz) [Longuet-Higgins 1950, Bonnefoy-Claudet et al. 2006, Peck 2008, Vassallo et al. 2012]. In particular, Withers et al. [1996] demonstrated that there is a strong correlation between wind speed and seismic background noise at seismological stations installed both in free-field and in bore-hole at different depths; they found that wind speed has a significant role in increasing seismic noise amplitude, especially at the surface, when it exceeds a threshold value of about 10 km/h. In our analysis, we looked at daily average wind speeds given by four meteorological stations operating in the area of the test building (Figure 8). Data of wind speed at the four stations are taken from http://www.agricoltura.regione.campania.it. These data were used to select calm and disturbed (in a meteorological sense) time intervals. To study daily variations, measurements of the building vibrations in the day and in the night were selected as being representative of calm and disturbed (in terms of traffic and working activities) time intervals, respectively.

In order to assess the influence of anthropic activities and meteorological disturbances in exciting building vibrations, we have compared the seismic signals during calm and disturbed time windows of seismic noise. In particular, daily variations were investigated by comparing the FASs of day- and night-records in calm weather conditions (panel a in Figure 9). The effects of meteorological perturbations were investigated by comparing the spectra of night-records characterized by low- and high- wind speed (panel b in Figure 9). We also computed the noise FASs recorded in the most critical condition, i.e. when both anthropic activities and weather perturbation attained high spectral levels (panel c in Figure 9).

For all the analyses, 30-min long records of seismic noise were subdivided into time windows of 60 sec each. For each of the 60-sec windows, the FAS was calculated for the three components of motion and a 0.5 Hz wide triangular smoothing operator was applied. Similarly, SSRs were computed through the smoothed spectra of each time window, and then averaged over the 30 min records. Figure 9 shows the average FASs for the three components of motion at stations D_2 and A_0, at the basement and at the second floor, respectively. Figure 10 shows the average SSRs with reference to station A_0 (H/H and V/V). In the following, we describe the observed similarities and discrepancies. However, an important feature emerging from Figure 9 is that, independently of the excitation type, never the reference station A_0 shows evidence of energy at

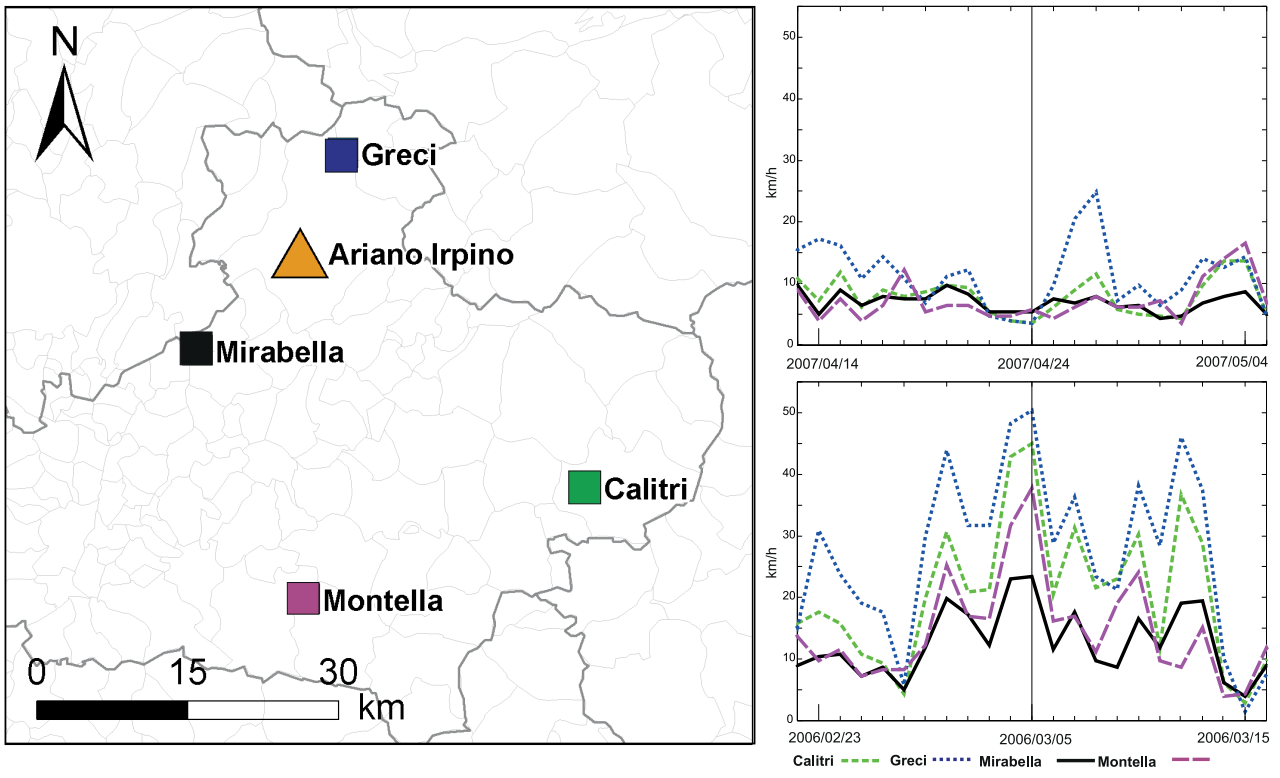

Figure 8. On the left side meteorological stations near Ariano Irpino; on the right side trends of daily-averaged wind speeds recorded during time intervals of low and high wind speed. The gray vertical lines represent day and hour of the noise sample selected for the analysis.

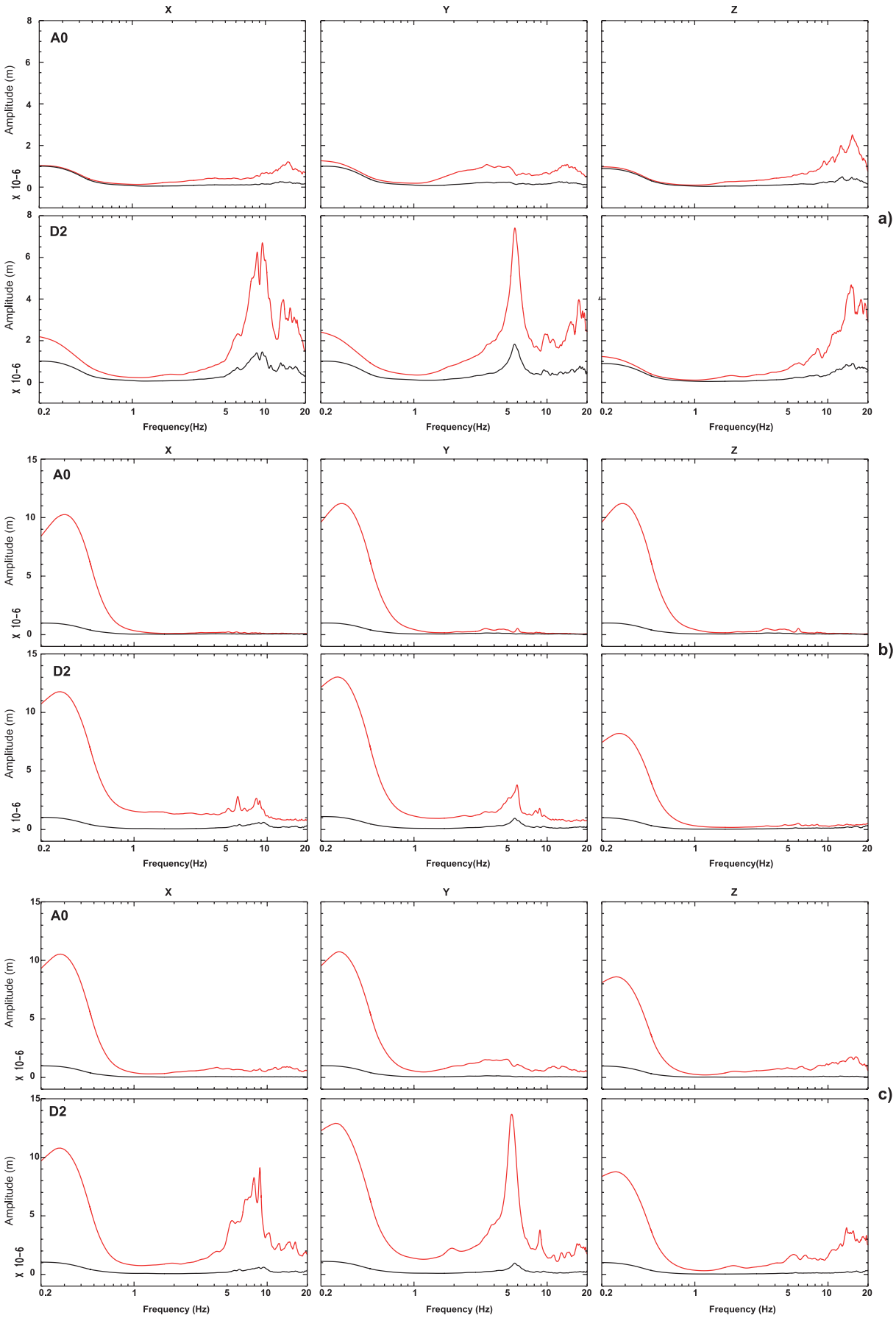

Figure 9. FAS variations at stations A0 (basement) and D2 (top); (a) influence of cultural noise, (b) influence of meteorological noise, (c) combination of both. The colour of plots indicates: (a) nightly (black curve) and daily recordings (red curve), (b) low wind speed (v ~ 5 km/h, black curve) and sustained wind (v ~ 25 km/h, red curve), (c) nightly recording with low wind speed (black curve) and daytime recording with high wind speed (red curve).

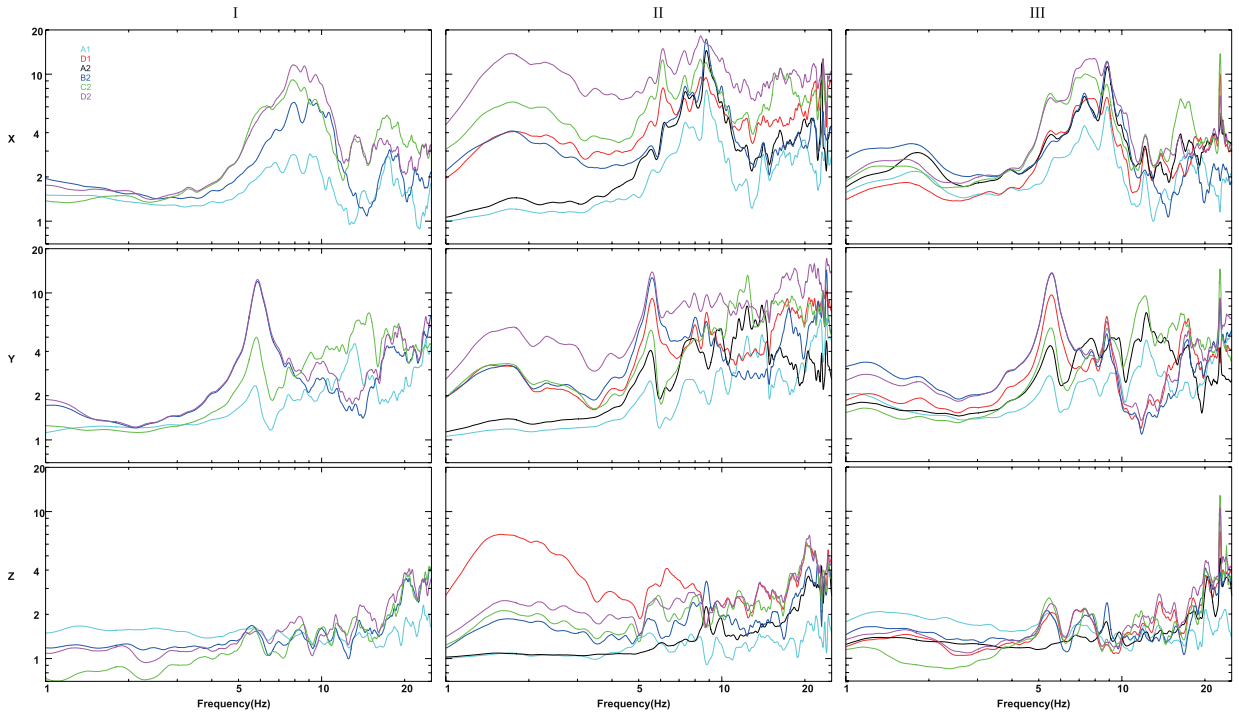

Figure 10. Average SSRs with respect to the reference station A0 computed using ambient noise recorded when (column I) the level of the daily anthropic activities is high, (column II) when the wind speed is high, and (column III) when both are high.

the frequencies that resonate at the higher stations. This is a strong indication that the amount of energy that is transmitted by the building to the ground is not significant and the basement record is a satisfactory representation of the incident seismic input.

5.1 Daily and meteorological variations

The differences in spectra between daily and nightly hours are illustrated in Figure 9a. This comparison uses noise data recorded in a day perturbed not so much by wind (wind speed < 7 km/h at the four meteorological stations). Figure 9a shows that the curves during the day increase in amplitude, as expected in relation to human activities both inside and outside the building. For the reference station A_0, the daily variation is fairly small up to about 10 Hz (no more than a factor of 2) but attains a factor of 3 to 4 for the vertical component at higher frequencies. Station A_0, located at the basement, shows an increase of the amplitude level of noise at high frequencies (above 1 Hz) caused by traffic during the daytime [according to Bonnefoy-Claudet et al. 2006]. At the highest floor, amplitude differences between day and night are more significant, reaching a relative factor of 4 for the two horizontal components at the station D2. Furthermore, the amplitudes of the horizontal components predominate over the vertical one in the frequency band 5 to 10 Hz, where the main vibration modes of the building fall. In particular, around the fundamental frequency between 5 and 6 Hz, the y component amplitude exceeds the vertical one by a factor of about 7. The x component also exceeds by about four times the vertical one at frequencies from 8 to 9 Hz. At low frequencies (f <2 Hz; Figure 9a) daily variations of the horizontal components at station D2 are greater than those of the reference station A_0. This could be due to localized sources of vibrations in this frequency band that are stronger in the building body and at the highest floors, where the Municipality offices are housed.

To study variations due to weather conditions (Figure 9b), we compared two time windows with wind speed of about 25 and 5 km/h, both recorded in the night in order to minimize the effect of anthropic activities. The estimated speed values are an average over the four meteorological stations. Again, the shapes of the spectra for the three components of motion are similar and, as expected, differences in amplitude for both stations are much more pronounced at low frequencies (f <1 Hz), where they attain a factor of 7. The marked difference in amplitude between calm and disturbed time windows, involving all the components of motion, suggests that periods with very strong meteorological disturbances can bias ambient noise measurements in buildings.

Figure 9c shows the amplitude levels for two noise recordings, the former taken in hours of high working activity with bad weather conditions, the latter in the night in a meteorologically calm period. The comparison clearly shows the combined effects of the two types of disturbances: at low frequencies (f <1 Hz) meteoro-

logical perturbations produce an amplification factor of about 8 - 9 for the three components of motion on both stations, at high frequencies (4 - 20 Hz) anthropic activity is predominant and affects to a higher extent the horizontal components.

5.2. Comparison between transfer functions inferred from earthquakes and ambient vibrations

In order to check the similarity of building responses in terms of resonant frequencies inferred from weak motions of earthquakes and ambient vibrations, we have first computed the transfer functions (1) for ambient vibrations in both cases where anthropic and meteorological sources predominate, then we compared SSRs using ambient noise with the earthquake results. Figure 10 shows SSRs computed when the level of the daily human activities is high (column I), when the wind speed is high (column II), and when both quantities are high (column III). Although the trend of transfer functions of the three components of motion shows some differences, they tend to reproduce fairly well the frequency of the first modes. Particularly for the y component, the match in the resonance frequency among the three cases is very good for all of the stations. Also the positions of the other first peaks are reproduced with sufficient accuracy, even in terms of amplification factors. For frequencies below 3 Hz, the transfer functions of ambient vibrations do not reproduce the expected tendency to unity toward zero frequency. This is observed for all stations on both horizontal components especially in presence of high wind speed (column II), and might be due, in addition to the wind action on the building as a whole, also to the fact that the velocity-transducers were not fixed to the floor but were simply placed on it. Therefore, in perturbed weather conditions their body and cables might have been shaken by wind, in addition to the building oscillation. The risk of a direct action of wind gusts on the body of sensors and cables is particularly high for stations located in places of the building not protected from the wind, such as terraces or balconies. To test this possi-

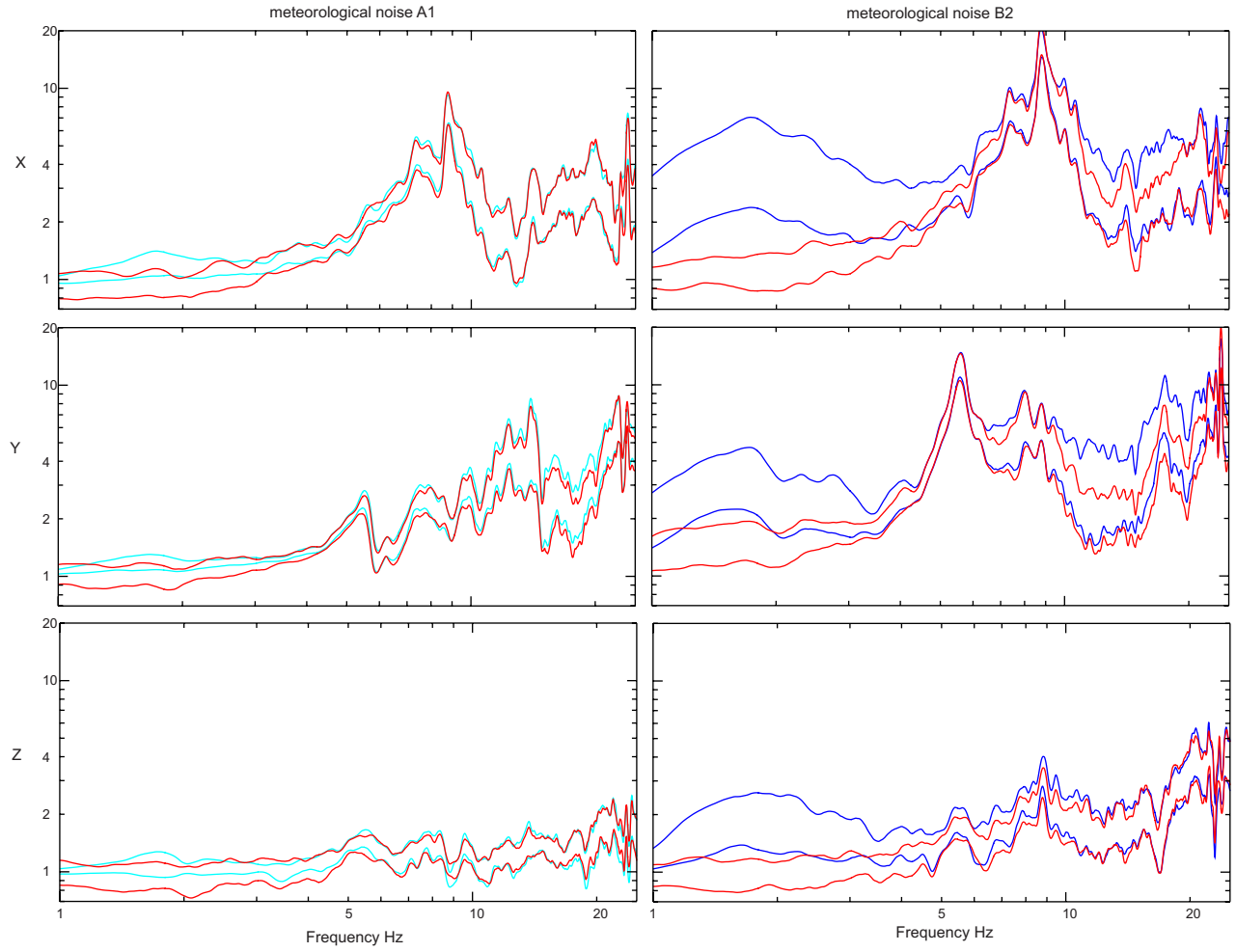

Figure 11. SSRs ±1 standard deviation of stations A1 (column I) and B2 (column II) in case of high wind speed. We overlaid the bands of uncertainties computed using recordings from velocimenters (light blue and dark blue curves for A1 and B2, respectively) to the same bands computed using recordings from accelerometers (red curves for both A1 and B2). Using the accelerometer data, the SSR bumps below 3 Hz disappear for the three components of motion.

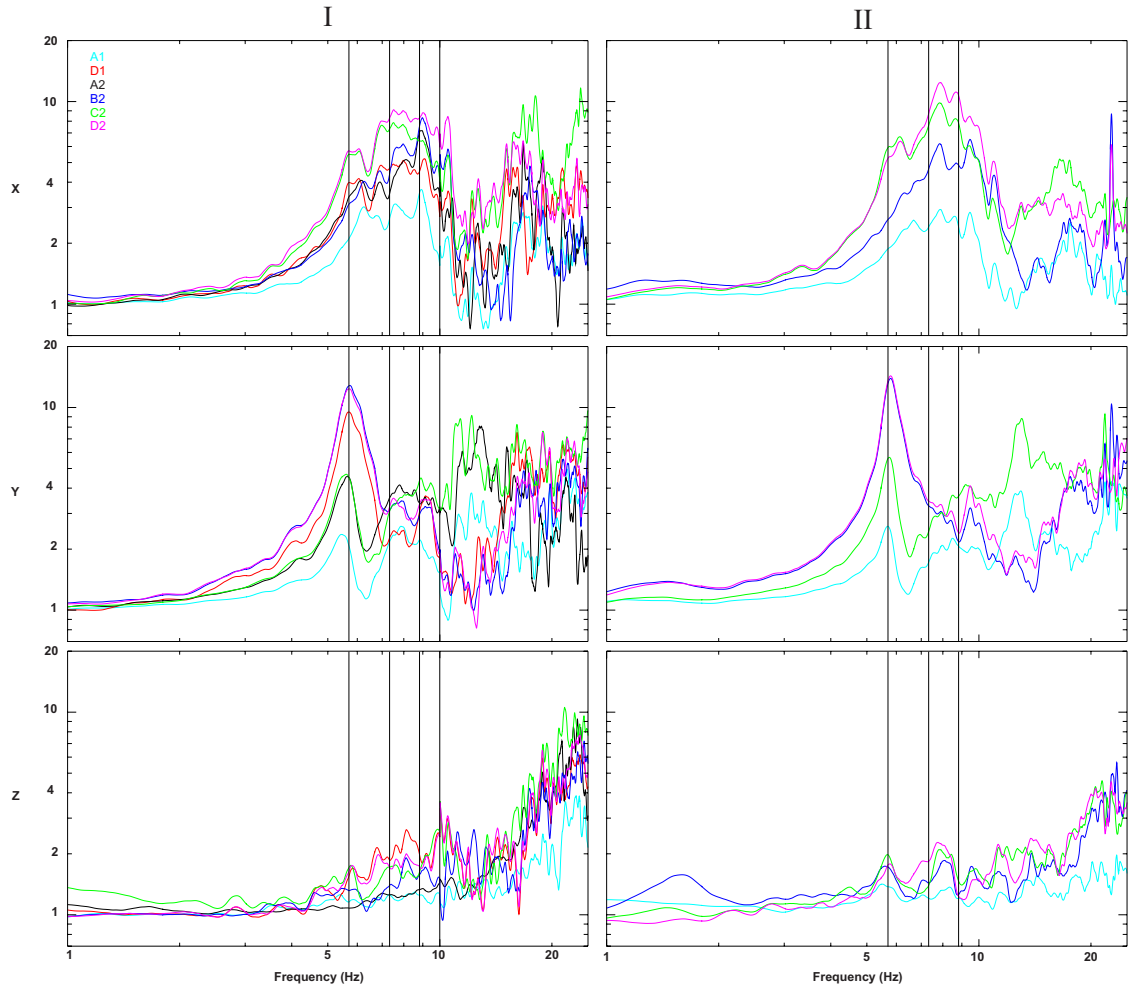

Figure 12. Average SSRs from (column I) earthquakes, and (column II) from noise recordings taken in conditions of low wind speed and minimum human activities.

ble origin of the low-frequency anomaly, we reproduced the curves in Figure 10 using recordings from accelerometers (Figure 11), which were mounted on metal bases firmly fixed to the building, and we found that the anomalous bumps below 3 Hz disappear.

Finally, Figure 12 shows the comparison between average SSRs obtained from earthquakes and those obtained from ambient noise when wind speed is low and human activities are minimum. In this ideal case, the SSR bumps below 3 Hz observed in presence of high wind (see Figure 10 columns II and III) do not occur, and the average SSRs derived from noise better reproduces those from earthquakes, even at low frequencies.

6. Discussion and Concluding Remarks

The combined use of earthquakes recordings and numerical modelling allowed us to interpret the seismic response of the study building in the linear domain. In general, numerical modelling are not able to reproduce all the resonant frequencies obtained from experimental data with high accuracy [Lin et al. 2005, Liu et al. 2005]. In this paper we have found a satisfactory agreement between experimental data and models for the first vibrational modes, including two translational modes and a rotational mode, with an acceptable outlining of vibration modes along the vertical axis (Table 4).

The values of the frequencies of the first modes are well reproduced by modelling, but some elements of discrepancy are also present between the actual behaviour of the building and simulations. For example, Figures 4 and 5a show a different behaviour of the pairs of stations A2, B2 and C2, D2, located at the same elevation, which is not fully reflected in numerical modelling. With referring to Figure 5a, A2 and C2 show amplification factors of the first vibration mode much smaller than those of the pair B2, D2. This likely derives from the fact that the side of the building facing south-west, that contains A2 and C2, is less free to oscillate with respect to the opposite side because of the presence of an adjoining building that tends to partially limit its horizontal motion; this is not taken into account by numerical modelling (Figure 5b),

which does not work so well for the couple of stations A2, C2. The actual response of the target building is certainly more complex than what the numerical model can reproduce, also considering the adjacent structures not considered in our simplified modeling.

The differences between the actual building behaviour and our numerical simulations confirm the difficulty in reproducing the details of the seismic response of structures using simplified modelling. This is probably due to the simplifications intentionally introduced in the model, the structural complexity of the building and the lack of experimental tests on materials.

The identification of the spectral peaks by means of seismic recordings is equally effective when using ambient vibrations, as shown in Figure 12. The average SSRs (both H/H and V/V) with respect to a basement reference well match the fundamental modes of the structure even using ambient noise, both in terms of spectral peaks and amplification factors. The frequencies of the second and third modes also reproduce those outlined by modelling with enough accuracy.

To conclude, our analysis confirms the well know result that ambient vibrations are quite reliable to characterize the seismic response of a building especially when noise recordings are taken at night time and in periods with very low weather disturbances (Figure 12). In general, low-cost noise measurements taken in an expeditious way and performed by using a single station located on top of the building, can be affected by anthropic activities inside the building and meteorological disturbances. This requires special attention in the installation of the seismic equipment, and in discriminating local or global effects related to human activities or wind that can alter the results obtained in the assumption of an almost white noise.

References

Bard, P. Y. (1999). Microtremor measurements: A tool for site effect estimation?, State-of-the-art Paper, Proceedings of the Second International Symposium on the Effects of Surface Geology on Seismic Motion,Yokohama, Irikura, Kudo, Okada, and Sasatani (Editors), Balkema, 3, 1251-1279.

Bindi, D., B. Petrovic, S. Karapetrou, M. Manakou, T.. Boxberger, D. Raptakis, K. D. Pitilakis, and S. Parolai (2015). Seismic response of an 8-story RC-building from ambient vibration analysis, Bulletin of Earthquake Engineering, 13(7), 2095-2120.

Bonnefoy-Claudet, S., F., Cotton and P. Y. Bard (2006). The nature of noise wavefield and its applications for site effects studies: A literature review, Earth-Science Reviews, 79 (3-4), 205-227, doi:10.1016/j.earscirev.2006.07.004.

Borcherdt, R. D. (1970). Effect of local geology near San Francisco Bay, Bull. Seism. Soc. Am., 60, 29-61.

Brincker, R., L. Zhang, and P. Andersen (2001). Modal identification of output-only systems using frequency domain decomposition. Smart materials and structures, 10(3), 441.

Burjánek, J., G. Gassner-Stamm, V. Poggi, J. R. Moore and D. Fäh (2010). Ambient vibration analysis of an unstable mountain slope, Geophys. J. Int., 180, 820-828, doi: https://doi.org/10.1111/j.1365-246X.2009.04451.x.

Burjánek J., J. R. Moore, F. X. Yugsi-Molina and D. Fäh (2012). Instrumental evidence of normal mode rock slope vibration, Geophys. J. Int., 188, 559-569, doi: https://doi.org/10.1111/j.1365-246X.2011.05272.x

Celebi, M., and E. Şafak (1991). Seismic response of Transamerica building. I: Data and preliminary analysis, Journal of Structural Engineering, 117(8), 2389-2404.

Clinton, J. F., S. C. Bradford, T. H. Heaton and L. Favela (2006). The observed wander of the natural frequencies in a structure, Bull. Seism. Soc. Am. 96, 237-257. https://doi.org/10.1785/0120050052,

Cook, R. D., D. S. Malkus and M. E. Plesha (1989). Concepts and Applications of Finite Elements Analysis, 3rd Edition, John Wiley & Son, New York, N.Y.

Di Giulio, G., F. Cara, A. Rovelli, G. Lombardo and R. Rigano (2009). Evidences for strong directional resonances in intensely deformed zones of the Pernicana fault, Mount Etna, Italy, Journal of Geophysical Research, 114, B10308, DOI:10.1029/2009JB006393.

Fäcke, A., S. Parolai, S. M. Richwalski and L. Stempniewski (2006). Assessing the vibrational frequencies of the cathedral of Cologne (Germany) by means of ambient seismic noise analysis, Natural Hazards, 38, 229-236, doi:10.1007/s11069-005-8616-2.

Fäh, D., F. Kind and D. Giardini (2001). A theoretical investigation of average H/V ratios, Geophys. J. Int., 145, 535-549.

Gallipoli, M. R., M. Mucciarelli and M. Vona (2009). Empirical estimate of fundamental frequencies and damping for Italian buildings, Earthquake Eng Struct. Dyn. 38, 973-988, doi: 10.1002/eqe.878.

Gentile, C., and A. Saisi (2007). Ambient vibration testing of historic masonry towers for structural identification and damage assessment, Construction and Building Materials, 21(6), 1311-1321.

Guéguen, P., M. Langlais, P. Foray, C. Rousseau and J. Maurie (2011). A natural seismic isolating system: the buried mangrove effects , Bull. Seism. Soc. Am. 101(3), 1073-1080, doi: 10.1785/0120100129.

Guéguen, P. (2012). Experimental analysis of the seismic response of one base-isolation building according to different levels of shaking: example of the Martinique earthquake (2007/11/29) Mw 7.3, Bulletin of Earthquake Engineering, 10(4), 1285-1298.

Guéguen P., M. Langlais, S. Garambois, C. Voisin and I. Douste-Bacqué (2017). How sensitive are site effects and building response to extreme cold temperature ? The case of the Grenoble's (France) City Hall building, Bulletin of Earthquake Engineering, 15: 889. doi:10.1007/s10518-016-9995-3

Herak, M. and D. Herak (2010). Continuous monitoring of dynamic parameters of the DGFSM building (Zagreb, Croatia), Bull Earthquake Eng, 8, 657-669, doi: 10.1007/s10518-009-9112-y.

Ivanovic, S., M. D. Trifunac, E. I. Novikova, A. A. Gladkov and M. I. Todorovska (2000). Ambient vibration tests of a seven-story reinforced concrete building in Van-Nuys, California, damaged by the 1994 Northridge earthquake, Soil Dyn. Earthquake Eng. 19, 391-411.

Kohler, M. D., P. M. Davis, and E. Safak (2005). Earthquake and ambient vibration monitoring of the steel-frame UCLA Factor building, Earthquake Spectra, 21(3), 715-736.

Kotronis, P., C. Tamagnini and S. Grange (2013) Soil-Structure Interaction. Alert Doctoral School 2013, Chapter "Using strong and weak motion to identify the dynamic characteristics and the response of buildings considering soil-structure interaction" by Guéguen P.

Lermo, J. and F. J. Chávez-García (1994). Are microtremors useful in site response evaluation?, Bull. Seismol. Soc. Am. 84, 1350-1364.

Longuet-Higgins, M. S. (1950). A theory for the generation of microseisms, Phil. Trans. R. Soc., Ser A, 243, 1-35.

Lin, C. C., L. L. Hong, J. M. Ueng, K. C. Wu, and C. E. Wang (2005). Parametric identification of asymmetric buildings from earthquake response records, Smart Mater. and Struct. 14, 850-861, DOI: 10.1088/0964-1726/14/4/045.

Liu, H., Z. Yang, M. S. Gaulke (2005). Structural identification and finite element modeling of a 14-story office building using recorded data, Eng. Struct. 27(3), 463-473.

Masi. A. and M. Vona (2010). Experimental and numerical evaluation of the fundamental period of undamaged and damaged RC framed buildings, Bull Earthquake Eng (2010) 8:643-656, DOI: 10.1007/s10518-009-9136-3.

Michel, C., P. Guéguen, S. E. Arem, J. Mazars and P. Kotronis (2007). Full scale dynamic response of a RC building under weak seismic motions using earthquake recordings, ambient vibrations and modelling, arXiv preprint arXiv:0710.1205.

Michel, C., P. Guéguen, P. Lestuzzi and P. Y. Bard (2010). Comparison between seismic vulnerability models and experimental dynamic properties of existing buildings in France, Bull Earthquake Eng (2010) 8:1295-1307, DOI: 10.1007/s10518-010-9185-7.

Mucciarelli, M. and M. R. Gallipoli, (2007). Non-parametric analysis of a single seismometric recording to obtain building dynamic parameters, Ann. Geoph., Vol. 50, N. 2, 259-266.

Nakamura, Y. (1989). A method for dynamic characteristics estimations of subsurface using microtremors on the ground surface, Quart. Rept. RTRI. Japan30 , 25-33

NTC 2008 - Norme Tecniche per le Costruzioni 2008, attinge da: Eurocodice 6, Ordinanza del Presidente del Consiglio dei Ministri n. 3431 May 2005, Decreto Ministero dei Lavori Pubblici November 20, 1987.

Oliveira, C. S. and M. Navarro (2010). Fundamental periods of vibration of RC buildings in Portugal from in-situ experimental and numerical techniques, Bull Earthquake Eng (2010) 8:609-642, DOI: 10.1007/s10518-009-9162-1.

Panzera, F., G. Lombardo and R. Rigano (2011). Evidence of topographic effects analysing ambient noise measurements: the study case of Siracusa, Italy, Seismol. Res. Lett. 82(3), 385-391, DOI:10.1785/gssrl.82.3.385

Panzera, F., G. Lombardo, S. D'Amico and P. Galea (2013). Speedy Techniques to Evaluate Seismic Site Effects in Particular Geomorphologic Conditions: Faults, Cavities, Landslides and Topographic Irregularities, Engineering Seismology, Geotechnical and Structural Earthquake Engineering, InTech, 101-145. DOI: 10.5772/55439.

Parolai, S., A. Fäcke, S. M. Richwalski and L. Stempniewski (2005). Assessing the Vibrational Fre-

quencies of the Holweide Hospital in the City of Cologne (Germany) by Means of Ambient Seismic Noise Analysis and FE modelling, Natural Hazards 34, 217-230.

Peck, L. (2008). Overview of Seismic Noise and its Relevance to Personnel Detection, ERDC/CRREL TR-08-5, April 2008.

Pischiutta, M., F. Salvini, J. Fletcher, A. Rovelli and Y. Ben-Zion (2012). Horizontal polarization of ground motion in the Hayward fault zone at Fremont, California: Dominant fault-high-angle polarization and fault-induced cracks, Geophys. J. Int., 188(3), 1255-1272, DOI:10.1111/j.1365-246X.2011.05319.x

Pischiutta, M., A. Rovelli, F. Salvini, G. Di Giulio and Y. Ben-Zion (2013). Directional resonance variations across the Pernicana Fault, Mt. Etna, in relation to brittle deformation fields, Geophys. J. Int., 193(2), 986-996, doi:10.1093/gji/ggt031.

Poggi, V., L. Ermert, J. Burjanek, C. Michel and D. Fäh (2015). Modal analysis of 2-D sedimentary basin from frequency domain decomposition of ambient vibration array recordings, Geophys. J. Int., 200, 615-626, doi:10.1093/gji/ggu420.

Rigano, R., F. Cara, G. Lombardo and A. Rovelli, A. (2008). Evidence of ground motion polarization on fault zones of Mount Etna volcano, J. Geophys. Res.,113, B10306, doi: 10.1029/2007JB005574

Trifunac, M. D., M. I. Todorovska, and T.-Y. Hao (2001). Full-Scale experimental studies of soil-structure interaction: a review, Proc. 2nd U.S.-Japan Workshop on Soil Structure Interaction, Tsukuba City, Japan, 6-8 March 2001, 1-52.

Tucker, B. and J. King (1984). Dependence of sediment-filled valley response on input amplitude and valley properties, Bull. Seism. Soc. Am., 74, 153-165.

Vassallo, M., G. Festa and A. Bobbio (2012). Seismic Ambient Noise Analysis in Southern Italy, Bull. Seism. Soc. Am. 102, (2), 574-586, doi: 10.1785/0120110018.

Ventura, C. E., W. L. Finn, J. F. Lord and N. Fujita (2003). Dynamic characteristics of a base isolated building from ambient vibration measurements and low level earthquake shaking. Soil Dynamics and Earthquake Engineering, 23(4), 313-322.

Welch, P. D. (1967). The use of fast Fourier transform for the estimation of power spectra: a method based on time averaging over short, modified periodograms, IEEE Trans Audio Electroacoust 15:70-73

Withers, M. M., R. C. Aster, C. J. Young,and E. P. Chael (1996). High-Frequency Analysis of Seismic Background Noise as a Function of Wind Speed and Shallow Depth, Bull. Seism. Soc. Am., 86, (5), 1507-1515.

*Corresponding author: Gaetano Riccio
Istituto Nazionale di Geofisica e Vulcanologia, Contrada Ciavolone, Grottaminarda (Italy);
email: gaetano.riccio@ingv.it